Materials Research. 2022; 25:e20210620
DOI: https://doi.org/10.1590/1980-5373-MR-2021-0620

Mechanical Properties of Melt Textured $Y_{1-x}Pr_xBa_2Cu_3O_{7-\delta}$ Superconductor (x = 0.00 and 0.05)

Yuri Aparecido Opata[a], Gelson Biscaia de Souza[b], Alcione Roberto Jurelo[b], Pedro Rodrigues Jr[b], João Frederico Haas Leandro Monteiro[c]*, Ezequiel Costa Siqueira[c]

[a]Technical University of Denmark, Department of Energy Conversion and Storage, Frederiksborgvej 399, 4000 Roskilde, Denmark.
[b]Universidade Estadual de Ponta Grossa, Departamento de Física, Av. Gen. Carlos Cavalcanti 4748, 84.030-000, Ponta Grossa, PR, Brasil.
[c]Universidade Tecnológica Federal do Paraná, Campus Ponta Grossa, Avenida Monteiro Lobato 1787, 84.016-210, Ponta Grossa, Paraná, Brasil.

Received: December 16, 2021; Revised: April 25, 2022; Accepted: May 11, 2022

This work reports the mechanical properties of *ab* and *a(b)c*-plane of melt textured $Y_{1-x}Pr_xBa_2Cu_3O_{7-\delta}$ (x = 0.00 and 0.05) superconductor. $Y_{1-x}Pr_xBa_2Cu_3O_{7-\delta}$ have been prepared by top seeding technique. Hardness and elastic modulus were obtained by instrumented indentation. Independent of the plane, the hardness values were around 5.0-7.5 GPa. Young's modulus was approximately the same for both samples for *ab*-plane, around 132 GPa at the deepest tip penetration. However, for *a(b)c*-plane, the value of Young's modulus for x = 0.05 is higher than observed for x = 0.00 sample.

Keywords: *Superconductor, YBCO, PBCO, Mechanical Properties, Hardness, Elastic modulus.*

1. Introduction

Since the beginning of studies in high critical temperature superconductors, one undesirable property has been the presence of granularity in sintered $YBa_2Cu_3O_{7-\delta}$ (Y - 123) material. To overcome this problem, a top-seeding melt texture growth (TSMTG) process was introduced[1,2]. With this process, it was possible to fabricate large single grains without high-angle grain boundaries in the $YBa_2Cu_3O_{7-\delta}$ matrix[3], which also contains small dispersed particles Y_2BaCuO_5 (Y - 211)[4] and usually a small addition of CeO_2[5,6]. In melt textured samples, the *c*-axis direction is well defined, while *a*- and *b*-axis directions are highly interchanged because of twinning.

Most of the orthorhombic $REBa_2Cu_3O_{7-\delta}$ (RE = Rare Earth elements) compounds exhibit superconductivity with critical temperature T_C above 90 K. The exceptions to this behavior are the elements Ce, Pr, and Tb. The suppression of superconductivity for $Y_{1-x}Pr_xBa_2Cu_3O_{7-\delta}$ occurs with increasing x, and superconductivity disappears with concomitant loss of metallic conductivity at $x > 0.6$[7]. For $PrBa_2Cu_3O_7$ (Pr - 123), the compound is non-metallic and non-superconducting, an antiferromagnetic insulator. Many models have been proposed to explain the disappearance of superconductivity in Pr, such as hole filling, magnetic pair breaking, hole localization, percolation, and so on[8-11], but the question of non-superconductivity in Pr - 123 is still open.

The interest in the praseodymium-containing YBCO system dated from the 1990s, when studies had already demonstrated the dependence of elastic properties with temperature and the Pr amount in polycrystals[12]. Ivanov et al.[13] studied elastic properties of granular $Y_{1-x}Pr_xBa_2Cu_3O_{7-\delta}$ with $0 > x > 0.45$ (superconducting) and $x = 0.65$ (nonsuperconducting), employing an ultrasonic pulse-echo technique during heating from cryogenic temperatures to the room temperature. The shear velocity $v = \sqrt{G/\rho}$, where G is the shear modulus and ρ the density, decreases with the increasing temperature for the same x, while, for the same temperature, it also decreases with increasing x. They observed anomalies in the shear modulus concerning stoichiometry and temperature. The authors indicated that the study of single crystals could bring insights to explain the observed variations in elastic properties with the Pr concentration in the material[13]. The melt-texturing of REBCO arose as a possible technique for producing large-grain materials on an industrial scale, aiming at applications in engineering devices such as energy-storage systems and motors. However, the mechanical performance was always a concern due to the intrinsic brittleness and high density of crystal defects of the RE-123 system[14].

In this scenario, single crystal study can help understand the basic mechanical behavior of melt textured yttrium-based materials. Variables such as hardness and elastic modulus of insulating/superconducting $Y_{1-x}Pr_xBa_2Cu_3O_{7-\delta}$ are of interest aiming at applications in electronic devices such as superconductor-insulator-superconductor junctions. In this study, we produced and characterized $Y_{1-x}Pr_xBa_2Cu_3O_{7-\delta}$ with different contents of Y and Pr. As a transition occurs from the superconductor state to an antiferromagnetic insulator one at $x \cong 0.56$, then we decided to produce a sample with a low Pr concentration (around 5%) to avoid undesired effects. The mechanical properties were measured by an instrumented indentation on *ab*- and *a(b)c*-planes. All analyzes are based on single samples.

*e-mail: jfhlmonteiro@hotmail.com

2. Experimental Details

$Y_{1-x}Pr_xBa_2Cu_3O_{7-\delta}$ superconductor pellets (x = 0.00 and x = 0.05) have been prepared by top seeding technique using melt-textured $NdBa_2Cu_3O_7$ seeds. Firstly, a ceramic sample was prepared by the conventional solid-state reaction method. Appropriate amounts of Y_2O_3, Pr_6O_{11}, $BaCO_3$, and CuO were mixed and calcinated in the air at 880 °C, 900 °C, and 920 °C for 24 hours and then slowly cooled up to 700 °C. For the melt textured samples, the starting composition was 75 wt % $Y(Pr)Ba_2Cu_3O_{7-\delta}$ + 25 wt % Y_2BaCuO_5 + 1 wt % CeO_2. Commercial powder Y_2BaCuO_5 was employed in the synthesis. Also, it was used CeO_2 addition to avoid the Y_2BaCuO_5 coarsening[5,6]. The mixture, in appropriate quantities, was pressed into cylindrical pellets, and a seed crystal of $NdBa_2Cu_3O_{7-\delta}$ was placed on the top of the pellet. Then, the temperature was increased to 920 ^{0}C at a rate of 40 ^{0}C/h and maintained in this condition for 24 h. After that, the temperature increased above the peritectic temperature, at around 1040 °C for x = 0.00 and 1045 °C for x = 0.05, and maintained for 3 h. Then, the temperature was quickly decreased in 0.1 h (6 minutes) within a temperature window of approximately 40 °C (45 °C) for the initiation of sample growth. The next step was the temperature decreasing at 0.5 °C/h up 980 °C. Then, the temperature was slowly cooled to 700 °C up to the ambient temperature. Finally, the melt textured samples were heated in flowing oxygen at 420 °C for 120 h. Figure 1 illustrates the temperature ramps, and Figure 2 shows a real photograph of the samples.

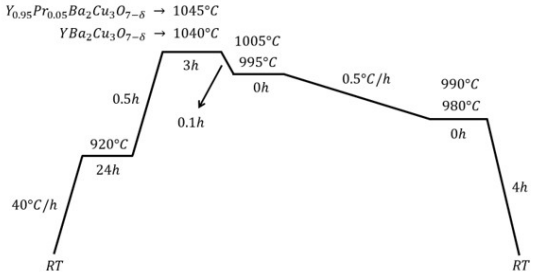

Figure 1. Temperature ramp diagram for sample texturing.

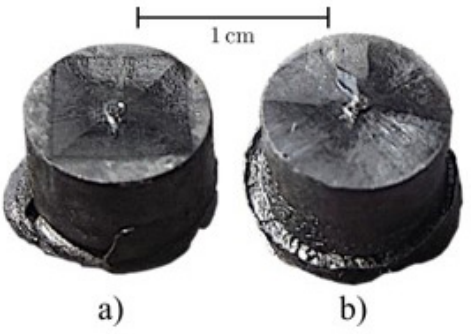

Figure 2. Real photograph of samples a) $Y_{0.95}Pr_{0.05}Ba_2Cu_3O_{7-\delta}$ and b) $YBa_2Cu_3O_{7-\delta}$. The samples are about 12 mm in diameter.

The single-phase formation of $Y_{1-x}Pr_xBa_2Cu_3O_{7-\delta}$ was confirmed by X-ray analysis, using a Shimadzu Ultima IV diffractometer with CuK_α radiation in θ-2θ configuration. The X-ray diffraction patterns were collected from 3º < 2θ < 120º with 0.02º steps and 3.5 s counting time. The microstructure and the growth process were analyzed by scanning electron microscopy (SEM) with energy-dispersive spectroscopy (EDS). Before the surface mechanical tests, samples were previously grounded and polished up to 1 μm diamond paste. Nanoindentation tests on $Y_{1-x}Pr_xBa_2Cu_3O_{7-\delta}$ samples were performed using a Nanoindenter XP™ and a diamond Berkovich-type indenter, with applied loads ranging from 10 to 300 mN in a 5 x 4 indentation matrix parallel and perpendicular to the *c*-axis. The loading-unloading curves consisted of 10 cycles with a loading time of 10 s and a holding time of 15 s. The distance between each indentation was 50 μm. The indentations were performed in pieces taken from the central region of the sample, thus avoiding regions with excess green phase (Y-211) and other impurities. Care was taken to perform the indentations in a region free of pores and cracks, and the mechanical properties near the surface and inside the grains could be measured. The *H* and *E* were determined following the Oliver and Pharr method[15].

3. Results and Discussion

The structure of the samples was investigated using X-ray diffraction. Figure 3 presents the diffractogram of the melt textured superconductor $YBa_2Cu_3O_{7-\delta}$ and $Y_{0.95}Pr_{0.05}Ba_2Cu_3O_{7-\delta}$ taken at room temperature. The measurements demonstrate that the pattern for the $Y_{0.95}Pr_{0.05}Ba_2Cu_3O_{7-\delta}$ is identical to that of $YBa_2Cu_3O_{7-\delta}$, showing that the two samples have the same orthorhombic structure. Also, the lattice parameters *a*, *b*, *c,* and *V* obtained from both samples indicated that the Pr atoms were substituted by Y atoms, in agreement with other studies[16].

The microstructure of the (a)-(b) $YBa_2Cu_3O_{7-\delta}$ and (c)-(d) $Y_{0.95}Pr_{0.05}Ba_2Cu_3O_{7-\delta}$ superconductor for *ab*- and *a(b)c*-planes is shown in Figure 4. From SEM-EDS, it was possible to analyze the composition of the superconducting matrix, the dispersion,

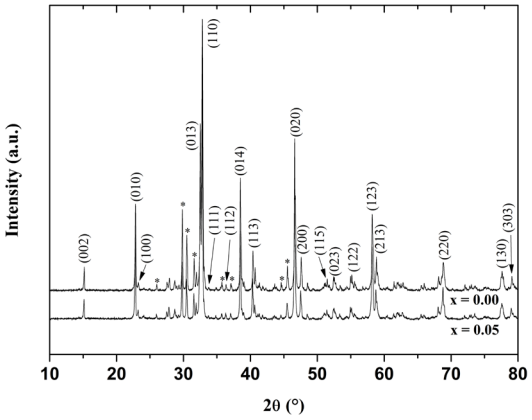

Figure 3. X-ray diffractogram of the melt textured $YBa_2Cu_3O_{7-\delta}$ and $Y_{0.95}Pr_{0.05}Ba_2Cu_3O_{7-\delta}$ superconductor was taken at room temperature. The corresponding number of PDF card for $YBa_2Cu_3O_{7-\delta}$ is 2101545. (*) corresponds to Y-211 phase.

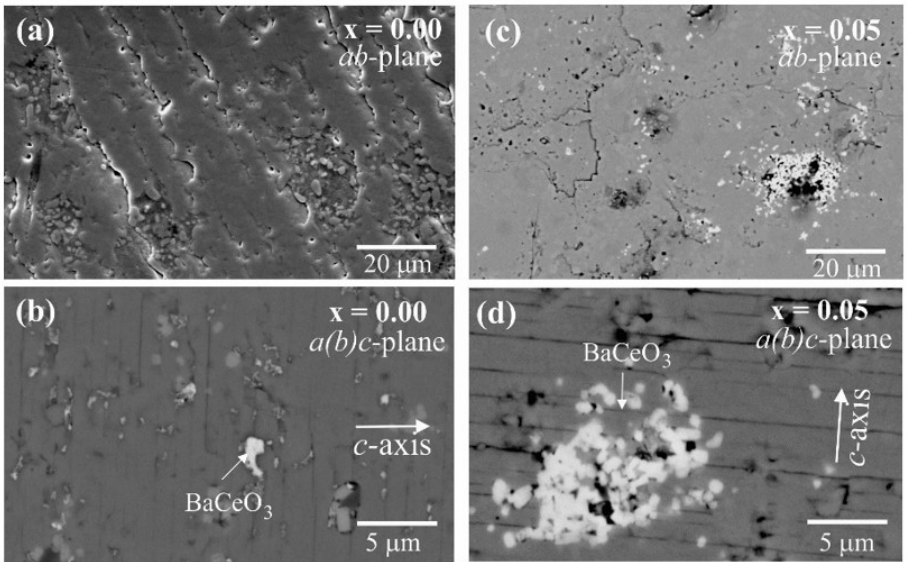

Figure 4. SEM micrographs of (a-b) $YBa_2Cu_3O_{7-\delta}$ and (c-d) $Y_{0.95}Pr_{0.05}Ba_2Cu_3O_{7-\delta}$melt-textured superconductor for *ab*- and *a(b)c*-planes.

and the composition of the Y_2BaCuO_5/Pr_2BaCuO_5 particles (211). It was observed that the superconducting matrix (123 phase) is strongly enriched with yttrium while that 211 particles (around 5 μm sizes) have intermediate quantities. It is known that the solubility of rare earth (RE) ions in the superconducting matrix increase with increasing RE ionic size, while the 211 particles embedded in the matrix will be poor in Pr[17,18]. A random distribution of $BaCeO_3$ particles between 1 and 5 μm in diameter are homogeneously dispersed within the $Y_{0.95}Pr_{0.05}Ba_2Cu_3O_{7-\delta}$. However, the granular nature and the porosity are clearly shown. Defects such as pores are created during the heating and cooling steps or formed during the oxygenation process. Also, as shown in panels (b) and (d), it was revealed microcracks parallel to (001) planes. The bulk critical temperatures for these samples are 91.7 K and 88.7 K for $YBa_2Cu_3O_{7-\delta}$ and $Y_{0.95}Pr_{0.05}Ba_2Cu_3O_{7-\delta}$ superconductors, respectively[19]. Further details on the sample preparation and characterization may be found in Reference[19,20].

Figure 5 shows a SEM image of indentions produced with ten loading cycles, from 10 to 300 mN on the melt textured $YBa_2Cu_3O_{7-\delta}$ superconductor and the corresponding loading curves. At the highest applied load of 300 mN, the maximum depth reached by the tip was around 1500-1700 nm in *ab*- and *a(b)c*-planes. For this x = 0.00 sample, curves were continuous, presenting no pop-ins caused by cracks nucleation or pores crushing. No *radial cracks* emanating from the corners of the indentation were observed. However, in both planes, notably in the *ab*-plane, it was possible to observe more material displaced around the tip imprint due to the nucleation and propagation of *lateral cracks*. The material displacement in successive indentation tests is a phenomenon typically observed in lamellar-like materials[21,22]. Generally, when these lateral cracks are nucleated, radial cracks are suppressed. However, the involved mechanisms seem to depend on specific features of the compound.

The analyses of the imprints morphologies shown in Figure 5 suggest that the plastic deformation mechanism is similar to that proposed by Pimentel et al.[21]. They studied the mechanical properties of the highly oriented $FeSe_{0.5}Te_{0.5}$ superconductor compound. The samples' morphology also consisted of plate-like crystals with a lamellar-like structure and the same behavior of cracking for the *ab*-plane as observed in this material. According to the authors, as the indenter penetrates in the *ab*-plane, cracks parallel to the surface are nucleated at the edges of the indenter, lifting material at the tip edges and eventually leading to the surface´s partial detachment (as seen in Figure 5a). In this mechanism, the crack pattern is assumed as perpendicular to the *c*-axis.

Figure 6 shows SEM images of indentions produced with ten loading cycles, from 10 to 300 mN on the melt textured $Y_{0.95}Pr_{0.05}Ba_2Cu_3O_{7-\delta}$ superconductor in the *ab*- and *a(b)c*-planes and the corresponding loading curves. At the highest applied load of 300 mN, the maximum depth reached by the tip was around 1450-1750 nm. For the *ab*-plane, the curve is not continuous, presenting tip incursions in the 1300 nm depth range. During the tests, the indenter is submitted to a triaxial stress distribution, and delamination can occur around the indenter, or lateral cracks can be nucleated, with the material being ejected by these tangential forces parallel to the surface. When this effect occurs, the indenter loss sustentation and penetration depth suddenly increase, reflecting in the loading curves as such discontinuities. In this material, as seen for the $YBa_2Cu_3O_{7-\delta}$, the material displacement around the tip imprint was also observed due to the nucleation and propagation of these cracks, again with a higher degree for *ab*-plane. No radial cracks emanating from the corners of the indentation were observed. To sum up, the surfaces morphologies after localized mechanical tests were alike between the x = 0.00 and x = 0.05 samples, although the latter disclosed intensified brittleness under normal loading.

Hardness profiles as a function of penetration depth for *ab*- and *a(b)c*-planes are presented in Figure 7 for

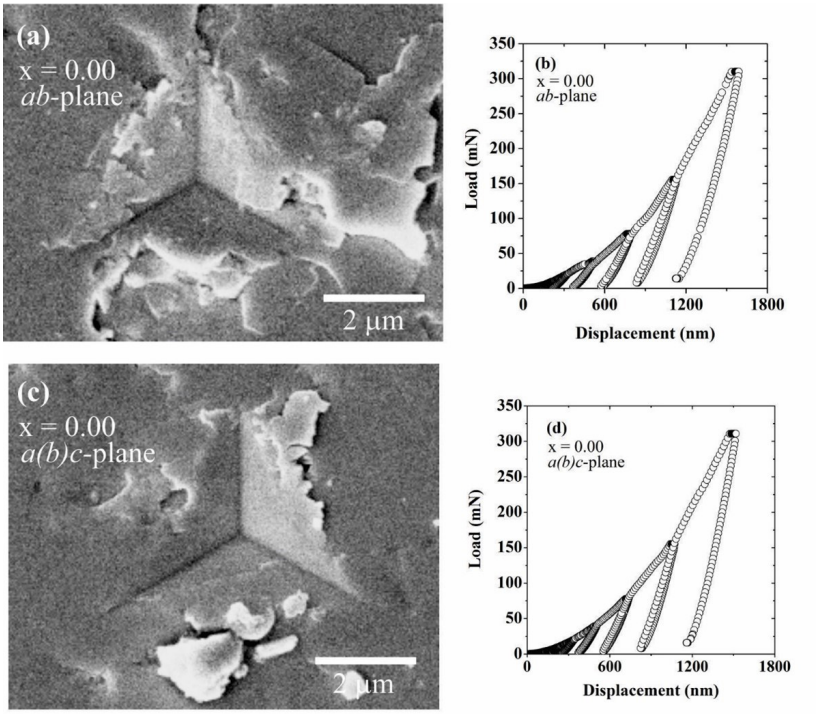

Figure 5. (a) and (c) Secondary-electrons scanning electron microscopy images of imprints produced with a Berkovich indenter under 300 mN load on the melt textured $YBa_2Cu_3O_{7-\delta}$ superconductor, in the *ab*- and *a(b)c*-planes, respectively; in (b) and (d), the corresponding loading-unloading curves related with the imprints shown in (a) and (c).

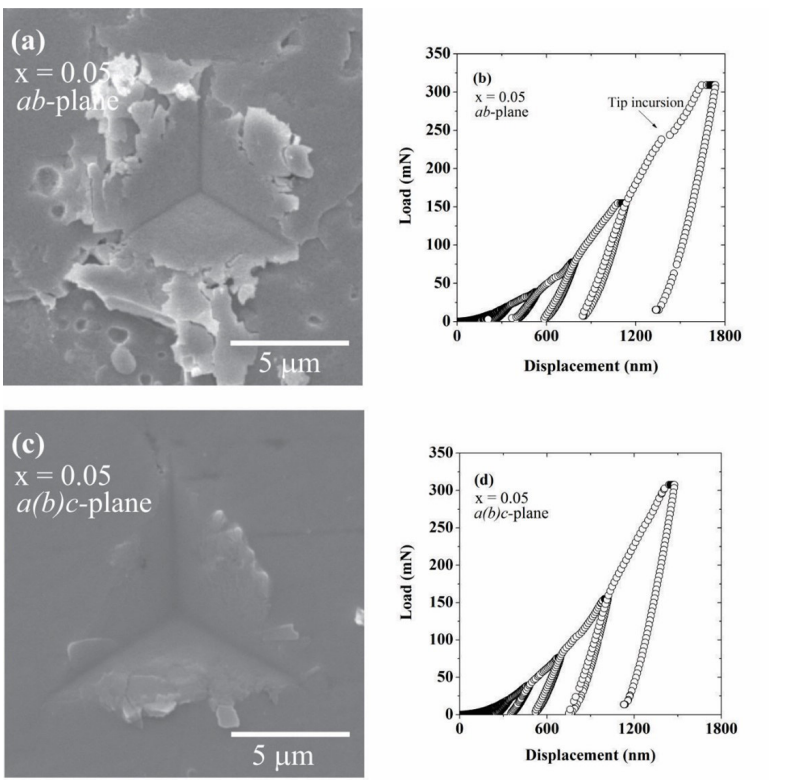

Figure 6. (a) and (c) Secondary-electrons scanning electron microscopy images of imprints produced with a Berkovich indenter under 300 mN load on the melt textured $Y_{0.95}Pr_{0.05}Ba_2Cu_3O_{7-\delta}$ superconductor in the *ab*- and *a(b)c*-planes, respectively; in (b) and (d), the corresponding loading-unloading curves related with the imprints shown in (a) and (c).

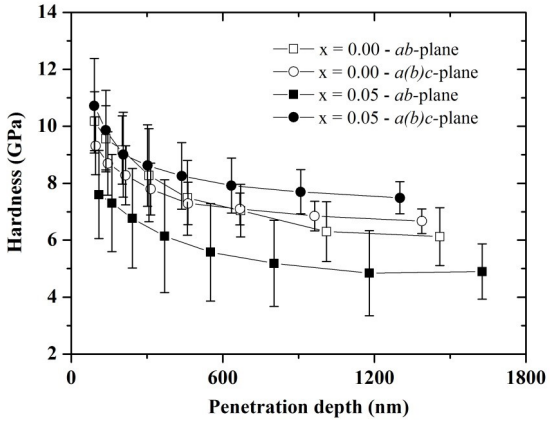

Figure 7. Hardness profiles as a function of penetration depth for *ab*- and *a(b)c*-planes of melt textured $YBa_2Cu_3O_{7-}\delta$ and $Y_{0.95}Pr_{0.05}Ba_2Cu_3O_{7-}\delta$ superconductor.

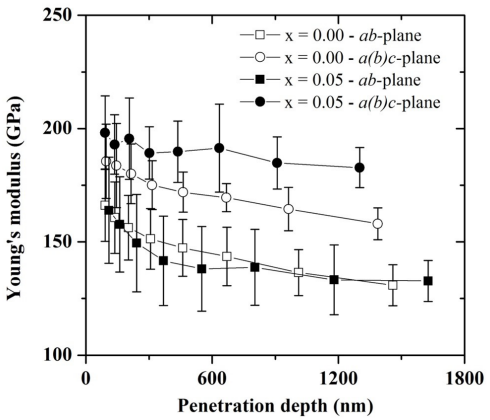

Figure 8. Elastic modulus profiles as a function of penetration depth for *ab*- and *a(b)c*-planes of melt textured $YBa_2Cu_3O_{7-\delta}$ and $Y_{0.95}Pr_{0.05}Ba_2Cu_3O_{7-\delta}$ superconductors.

x = 0.00 and x = 0.05 samples. All curves presented higher hardness values at low penetration depths and then decreased continuously in the analyzed penetration depth. Independent of the investigated plane or sample, the profiles tend to reach a plateau at deeper regions, around 5-7.5 GPa at approximately 1500-1700 nm. The x = 0.05 profile at the *ab*-plane was the lower one, explained by the fracture-promoted increase in the contact area during indentation, evidenced by tip-incursions as shown in Figure 6b. Note that the profiles are deeper than 200 nm (the tip rounding radius) to avoid errors in the contact area measurement, as well as the indentation size effect[23]. Nevertheless, others factors may originate the variation observed in hardness with penetration depth, as outermost plastic deformation layers produced by polishing, microcracking in adjacent lamellae, or the crushing of inner pores. Actually, such decrease was small compared to those observed in other lamellar-like single crystals[21,22] (it is in the order of the error bars), having little influence in the measurements.

Studying the indentation hardness H of $REBa_2Cu_3O_{7-\delta}$, researchers obtained values of 5 + 2 GPa for polycrystalline, 8.0 + 0.5 for single crystals and 9.0 + 0.5 GPa for both *ab*- and *a(b)c*-plane in melt-textured superconductor bulks[24]. The RE corresponds to a natural mixture of rare earth elements (Y – Yb – Dy – Ho – Tm – Lu – Gd – Tb – Sm – Ce – Eu – Nd) extracted from the xenotime mineral. In accordance with the authors, the different values for the hardness are due to the different microstructures present in these materials. The hardness of the polycrystalline $REBa_2Cu_3O_{7-\delta}$ is the lowest because pores collapse under indentation, leading to the tip incursion and the subsequent overestimation of the contact area (since $H \propto A^{-1}$). On the other hand, the highest value observed for the melt textured sample is due to the presence of the 211 precipitates, which are harder and stiffer than the 123 phase. The hardness of the 211 phase is 14 + 2 GPa, while it is about 10-11 GPa for the pure 123 phase. Values of the single crystal with lamellar-like structure, with a small size of approximately 1 mm and 20 μm thick (observed at the lamellar edges), were lower than those of the melt textured samples, explained by the specific deformation features of lamellar-like structures, as discussed previously in this report and in[21,22].

Figure 8 shows elastic modulus profiles as a function of penetration depth for *ab*- and *a(b)c*-planes of melt textured $YBa_2Cu_3O_{7-\delta}$ and $Y_{0.95}Pr_{0.05}Ba_2Cu_3O_{7-\delta}$ superconductor. Open and closed symbols, respectively, represent pure and doped samples. The elastic modulus was higher near the surface and decreased with the increasing penetration depth due to the aforementioned artifacts affecting indentation measurements. It is conspicuous that, differently from hardness, the planes present significant variations in elastic modulus. For *ab*-plane, the elastic modulus is approximately the same for x = 0.00 and x = 0.05 samples, around 132 GPa at the deepest tip penetration. However, for *a(b)c*-plane, the elastic modulus value for x = 0.05 is higher than that observed for the x = 0.00 sample, i.e., around 183 GPa and 147 GPa, respectively, both at the deepest tip penetration.

The ~24% increase in elastic modulus, attained by varying the stoichiometry from $YBa_2Cu_3O_{7-\delta}$ to $Y_{0.95}Pr_{0.05}Ba_2Cu_3O_{7-\delta}$, is possibly a consequence of different interactions experienced by neighboring atoms at the orthorhombic structure. The electrons distributions are Ba = [Xe] $6s^2$ and Pr = [Xe] $4f^3 6s^2$. Hence, substituting barium for praseodymium in the position of the rare earth atom introduces more electrons in the band structure. The consequences to the lattice parameters were minimal, as inferred from XRD results, shown in Figure 3. On the other hand, T_C varies from 91.7 K for $YBa_2Cu_3O_{7-\delta}$ to 88.7 K for $Y_{0.95}Pr_{0.05}Ba_2Cu_3O_{7-\delta}$ [19,20]. The potential energy among adjacent atoms also changes locally since the electron screening of the nucleus is stronger in Pr than it is in Ba. Such effect is more noticeable in the c direction, where the atomic density is higher from a RE atom´s point of view. The understanding of the mechanism through which the electron balance affects mechanical properties of the $REBa_2Cu_3O_{7-}\delta$ material is beyond the scope of this report. Nevertheless, variations in the potential energy U through the c-axis do result in different atomic bonding forces ($\mathbf{F} = -\nabla U$) and equilibrium separation r_0 in that direction. As a result, the elastic modulus varies as well, as measured here for the a*(b)*c-plane, since it strongly depends on bonding. From a simplified approach[25],

Table 1. Microscopic mechanical properties of $YBa_2Cu_3O_{7-\delta}$ and $Y_{0.95}Pr_{0.05}Ba_2Cu_3O_{7-\delta}$ compounds obtained from *ab*- and *a(b)c*- plane.

Compounds	plane	*H* (GPa)	*E* (GPa)	*H/E**
$YBa_2Cu_3O_{7-\delta}$	*ab*	6.1 ± 1.0	130.8 ± 9.0	0.04 ± 0.01
	a(b)c	6.7 ± 0.4	147.0 ± 7.1	0.04 ± 0.01
$Y_{0.95}Pr_{0.05}Ba_2Cu_3O_{7-\delta}$	*ab*	4.9 ± 1.0	132.7 ± 9.0	0.03 ± 0.01
	a(b)c	7.5 ± 0.6	182.8 ± 8.8	0.04 ± 0.01

$$E \approx \frac{1}{r_0}\left|\frac{d^2U}{dr^2}\right|_{r=r_0} \quad (1)$$

The elastic module of the pure $YBa_2Cu_3O_{7-\delta}$ sample measured at both planes agrees with literature data[24]. In $REBa_2Cu_3O_{7-d}$ superconductor single crystals, Foerster et al.[24] obtained 107 GPa for elastic modulus. The low value of *E* was attributed to the small sample thickness.

The plastic index is a useful correlation to compare mechanical properties of the $YBa_2Cu_3O_{7-\delta}$ and $Y_{0.95}Pr_{0.05}Ba_2Cu_3O_{7-\delta}$. It allows to predict a material´s wear behavior in service through the ratio H / E^*, where

$$E^* = E / (1 - n^2) \quad (2)$$

is the effective elastic modulus[26]. The efficiency of such parameters when applied in superconductor single crystals was demonstrated elsewhere[27]. Plastic indexes, summarized in Table 1, were calculated by assuming the Poisson´s ratio $\nu = 0.25$ for both compounds[28], and hardness *H* and elastic modulus *E* values inferred at the deepest penetration depths in Figures 7 and 8. In the *ab*-plane, the $x = 0.00$ condition disclosed a slightly higher index of plasticity; differently, similar values were obtained for *a(b)c*-planes of both compounds. Thus, the tribological strength is expected to depend neither the *x* value nor the single crystal´s plane. Interestingly, according to the Cheng and Cheng[26] results, such plastic index values situate $Y_{1-x}Pr_xBa_2Cu_3O_{7-\delta}$ in the same class than metals ($H / E^* < 0.3$), and far from typical brittle materials such as sapphire and fused silica.

4. Conclusions

The effects of Pr addition on mechanical properties of *ab*- and *a(b)c*-plane of melt textured $YBa_2Cu_3O_{7-\delta}$ superconductor have been studied. The samples were produced by top seeding technique and characterized regarding structural, morphology, and mechanical properties along the *ab*- and *a(b)c*-planes. All samples corresponded to the orthorhombic $YBa_2Cu_3O_{7-\delta}$ phase. The hardness of the samples was the same and independent of the plane, with values approximately between 5-7.5 GPa. For *ab*-plane, the elastic modulus was approximately the same in both samples, around 132 GPa. On the other hand, for *a(b)c*-plane, the value of elastic modulus for doped sample was higher than that observed for the pure sample, around 147 GPa and 183 GPa, respectively.

5. Acknowledgments

Authors are grateful to Prof. C. M. Lepienski for the use of nanoindenter, and the C-LABMU/UEPG for other characterization facilities. This work was partially financed by CNPq under contract n^0 472.746/2013-8.

6. References

1. Morita M, Takebayashi S, Tanaka M, Kimura K, Miyamoto K, Sawano K. Quench and Melt Growth (QMG) Process for Large Bulk Superconductor Fabrication. Adv Supercond. 1991;3:733.
2. Jin S, Tiefel TH, Sherwood RC, van Dover RB, Davis ME, Kammlott GW, et al. Melt-textured growth of polycrystalline $YBa_2Cu_3O_{7-\delta}$ with high transport J_c at 77 K. Phys Rev B Condens Matter. 1988;37:7850.
3. Jin S, Tiefel TH, Sherwood RC, Davis ME, van Dover RB, Kammlott GW, et al. High critical currents in Y-Ba-Cu-O superconductors. Appl Phys Lett. 1988;52(24):2074-6.
4. Mendoza E, Puig T, Varesi E, Carrillo AE, Plain J, Obradors X. Critical current enhancement in YBCO–Ag melt-textured composites: influence of microcrack density. Physica C. 2000;334(1-2):7-14.
5. Vilalta N, Sandiumenge F, Pinol S, Obradors X. Precipitate size refinement by CeO_2 and Y_2BaCuO_5 additions in directionally solidified $YBa_2Cu_3O_7$. J Mater Res. 1997;12(1):38-46.
6. Obradors X, Yu R, Sandiumenge F, Martinez B, Vilalta N, Gomis V, et al. Directional solidification of $ReBa_2Cu_3O_7$ (Re = Y, Nd): microstructure and superconducting properties. Supercond Sci Technol. 1997;10(12):884-90.
7. Neumeier JJ, Maple MB. Superconducting critical temperature and electrical resistivity of the system $Y_{1-x}Pr_xBa_2Cu_3O_{6.95}$ ($0 \leqslant x \leqslant 1$). Physica C. 1992;191(1-2):158-66.
8. Neumeier JJ, Bjornholm T, Maple MP, Schuller IK. Hole filling and pair breaking by Pr ions in $YBa_2Cu_3O_{6.95\pm0.02}$. Phys Rev B Condens Matter. 1989;63:2516.
9. Peng JL, Klavins P, Shelton RN, Radousky HB, Hahn PA, Bernardez L. Upper critical field and normal-state properties of single-phase $Y_{1-x}Pr_xBa_2Cu_3O_{7-\gamma}$ compounds. Phys Rev B Condens Matter. 1989;40(7):4517-26.
10. Fink J, Nucker N, Romberg H, Alexander M, Maple MB, Neumeier JJ, et al. Evidence against hole filling by Pr in $YBa_2Cu_3O_7$. Phys Rev B Condens Matter. 1990;42(7):4823-6.
11. Infante C, El Mously MK, Dayal R, Husain M, Siddiqi SA, Ganguly P. On the localisation of charge carriers and suppression of superconductivity by praseodymium in systems derived from YBa2Cu3O7−d. Physica C. 1990;167(5-6):640-56.
12. Lemmens P, Hunnekes C, Froning P, Ewert S, Passing H, Marbach G, et al. Elastic properties of $YBa_2Cu_3O_x$, $(Y_{1-y}Pr_y)Ba_2Cu_3O_7$ and $(BiPb)_2Sr_2Ca_2Cu_3O_{10}$ studied by ultrasound. J Less Common Met. 1990;164-165:1129-35.
13. Ivanov O, Fossheim K, Balankina E, Cjølmesli S, Nyhus J. Shear elastic properties of the $Y_{1-x}Pr_xBa_2Cu_3O_{7-\delta}$ system: A possible correlation between T_c and a structural instability. Phase Transit. 1999;70(3):147-59.
14. Lo W. Recent progress in large-grain REBCO melt texturing. J Miner Met Mater Soc. 2000;52(6):18-21.
15. Oliver WC, Pharr GM. An improved technique for determining hardness and elastic modulus using load and displacement sensing indentation experiments. J Mater Res. 1992;7(6):1564-83.
16. Radousky HB. A review of the superconducting and normal state properties of $Y_{1-x}Pr_xBa_2Cu_3O_7$. J Mater Res. 1992;7(7):1917-55.
17. Krauns C, Sumida M, Tagami M, Yamada Y, Shiohara Y. Solubility of RE elements into Ba–Cu–O melts and the enthalpy of dissolution. Z Phys B. 1994;96(2):207-12.

18. Qi X, MacManus-Driscoll JL. Liquid-phase epitaxial growth of $REBa_2Cu_3O_{7-\delta}$ (RE=Y, Yb, Er) thick films at reduced temperatures. J Cryst Growth. 2000;213(3-4):312-8.
19. Opata YA, Monteiro JFHL, Jurelo AR, Siqueira EC. Critical current density in $(YBa_2Cu_3O_{7-\delta})_{1-x}$ –$(PrBa_2Cu_3O_{7-\delta})_x$ melt-textured composites. Physica C. 2018;549:107-12.
20. Opata YA, Monteiro JFHL, Jurelo AR, Rodrigues P Jr. Fluctuation-induced conductivity in melt-textured Pr-doped $YBa_2Cu_3O_{7-\delta}$ composite superconductor. Phase Transit. 2018;91(4):343.
21. Pimentel JL Jr, Pureur P, Lopes CS, Serbena FC, Foerster CE, Silva SA, et al. Mechanical properties of highly oriented $FeSe_{0.5}Te_{0.5}$ superconductor. J Appl Phys. 2012;111:033908.
22. Souza GB, Serbena FC, Jurelo AR, Silva SA, Pinheiro LBLG, Dias FT, et al. On the determination of hardness and elastic modulus in $BaFe_2As_2$ lamellar-like material. J Mater Res. 2016;31(10):1413-22.
23. Fisher-Cripps AC. Nanoindentation. New York: Springer-Verlag; 2004.
24. Foerster CE, Serbena FC, Jurelo AR, Ferreira TR, Rodrigues P Jr, Chinelatto AL. Mechanical Properties of $REBa_2Cu_3O_{7-\delta}$ Superconductor With RE Obtained From Xenotime Mineral. IEEE Trans Appl Supercond. 2011;21(2):52-9.
25. Meyers M, Chawla K. Mechanical behavior of materials. 2nd ed. New York: Cambridge University Press; 2009. 145 p.
26. Cheng Y, Cheng C. Scaling, dimensional analysis, and indentation measurements. Mater Sci Eng Rep. 2004;44(4-5):91-149.
27. Souza GB, Jurelo AR, Monteiro JFHL, Oliveira WR, Barcote MV, Siqueira EC. BiS_2-based superconductor presents ductile-like tribo-mechanical behavior. Supercond Sci Technol. 2017;30:075005.
28. Diko P, Fuchs G, Krabbes G. Influence of silver addition on cracking in melt-grown YBCO. Physica C. 2001;363(1):60-6.